Impact of the various spin- and orbital-ordering processes on the multiferroic properties of orthovanadate $DyVO_3$

Q. Zhang,[1,2,*] K. Singh,[1,3] C. Simon,[4] L. D. Tung,[5] G. Balakrishnan,[5] and V. Hardy[1]

[1]*Laboratoire CRISMAT, UMR 6508, CNRS ENSICAEN, 6 Boulevard du Maréchal Juin, F-14052 Caen Cedex 4, France*

[2]*Ames Laboratory and Department of Physics and Astronomy, Iowa State University, Ames, Iowa 50011, USA*

[3]*UGC-DAE Consortium for Scientific Research, University Campus, Khandwa Road, Indore 452001, India*

[4]*Institut Laue Langevin, 6 rue Jules Horowitz, Boîte Postale 156, F-38042 Grenoble Cedex 9, France*

[5]*Department of Physics, University of Warwick, Coventry CV4 7AL, United Kingdom*

(Received 15 February 2014; revised manuscript received 23 May 2014; published 23 July 2014)

The orthovanadate $DyVO_3$ crystal, known to exhibit multiple structural, spin-, and orbital-ordering transitions, is presently investigated on the basis of magnetization, heat capacity, resistivity, dielectric, and polarization measurements. Our main result is experimental evidence for the existence of multiferroicity below a high T_C of 108 K over a wide temperature range including different spin-orbital-ordered states. The onset of ferroelectricity is found to coincide with the antiferromagnetic C-type spin-ordering transition taking place at 108 K, which indicates that $DyVO_3$ belongs to type-II multiferroics exhibiting a coupling between magnetism and ferroelectricity. Some anomalies detected on the temperature dependence of electric polarization are discussed with respect to the nature of the spin-orbital-ordered states of the V sublattice and the degree of spin alignment in the Dy sublattice. The orthovanadates RVO_3 (R = rare earth or Y) form an important new category for searching for high$-T_C$ multiferroics.

DOI: 10.1103/PhysRevB.90.024418 PACS number(s): 75.25.Dk, 75.85.+t, 75.50.Ee

I. INTRODUCTION

Multiferroic materials, with coexistence of magnetic ordering and ferroelectricity, have recently attracted immense attention, aimed both at studying the fundamental properties and at exploiting them in multifunctional device applications [1–3]. In conventional type-I multiferroics [4,5], the origins of the ferroelectric and the magnetic order are not related, which leads to weak magnetoelectric coupling. In contrast, the type-II multiferroics (related to the so-called spin-driven ferroelectricity) [6,7] usually exhibit a lower electric polarization, but the ferroelectricity is directly coupled to the magnetic order and therefore a strong intrinsic magnetoelectric coupling can be induced. To date, spin-driven ferroelectricity has been discovered in various systems, such as boracite $Ni_3B_7O_{13}Br$ [8], chromium chrysoberyl Cr_2BeO_4 [9], perovskite manganites $RMnO_3$ (R = Tb, Dy, Ho, Tm, and Y) [7], RMn_2O_5 (R = Tm, Ho, Dy, Tb, Y, and Er) [10–12], $Ni_3V_2O_8$ [13], $FeVO_4$ [14], $MnWO_4$ [15], $CoCr_2O_4$ [16], $FeCr_2O_4$ [17], FeV_2O_4 [18], $CuCrO_2$ [19], $CuBr_2$ [20], $RCrO_3$ (R = Sm, Gd, Tb, Er, and Tm) [21], CuO [22], $CaMn_7O_{12}$ [23], and $SmFeO_3$ [24,25], etc. [6,7]. It is known that the leakage is a major problem for measurement of ferroelectricity and for applications of high-temperature multiferroics. In this regard, it is beneficial if a multiferroic material could exhibit both a high ferroelectric critical temperature (T_C) and a very low dielectric loss ($\ll$0.1 [20]). On the other hand, if spin-driven ferroelectricity would occur in materials that exhibit several magnetic or orbital-ordering transitions, multiple anomalies in temperature dependence of electric polarization are expected to take place in different temperature windows. Such materials could thus provide good candidates to allow investigating the effect of different magnetic or orbital orderings on ferroelectricity in the same single-phase material. Therefore, it is of interest to search for novel spin-driven ferroelectric materials with high ferroelectric critical temperatures, very low dielectric loss, and successive/multiple anomalies in the ferroelectricity over a wide temperature region.

Compared to manganites with orbital-active e_g electrons, the perovskite-type vanadium oxides RVO_3 (R = rare earth elements and Y) with orbital-active t_{2g} electrons is another type of correlated electron system and may be expected to undergo a weaker Jahn-Teller interaction [26–28]. The relationship between spin, orbital, and lattice degrees of freedom in such systems is more subtle and complex than that observed in manganites. The RVO_3 compounds have a *Pbnm* orthorhombic lattice at room temperature and exhibit two distinct spin-ordering (SO) and orbital-ordering (OO) states depending on the R^{3+} ionic radius and/or temperature [27,29–32]. Interestingly, switching between these two spin/orbital-ordering states can be induced by external stimuli such as a magnetic field, when R is Dy or Ho [27]. All members of the RVO_3 family exhibit a structural transition at T_{OO1} (ranging from 150 to 200 K) from *Pbnm* orthorhombic to $P2_1/b$ monoclinic with G-type OO [see Fig. 1(a)]. In this G-type OO, one electron occupies the d_{xy} orbital, while another electron occupies the d_{yz} or d_{zx} orbitals that are staggered in all three spatial directions [27,29]. With decreasing temperature, all RVO_3 compounds exhibit a magnetic transition [27,30] at T_{SO1}, from the paramagnetic state to C-type SO. This ordering of the V^{3+} spins corresponds to an antiferromagnetic (AFM) alignment within the xy plane, together with a ferromagnetic alignment along the z axis, as shown in Fig. 1(a). The AFM Néel temperature (named T_{SO1} here) monotonously increases from 90 K (Lu) to 140 K (La) because of the enhancement of the spin and orbital exchange interactions between the nearest-neighbor V sites induced by decreasing V-O-V bond angle distortion with increasing ionic radius [27]. It turns out that $DyVO_3$ is located at the vicinity of the boundary (1.09 Å)

*Corresponding author: qzhangemail@gmail.com

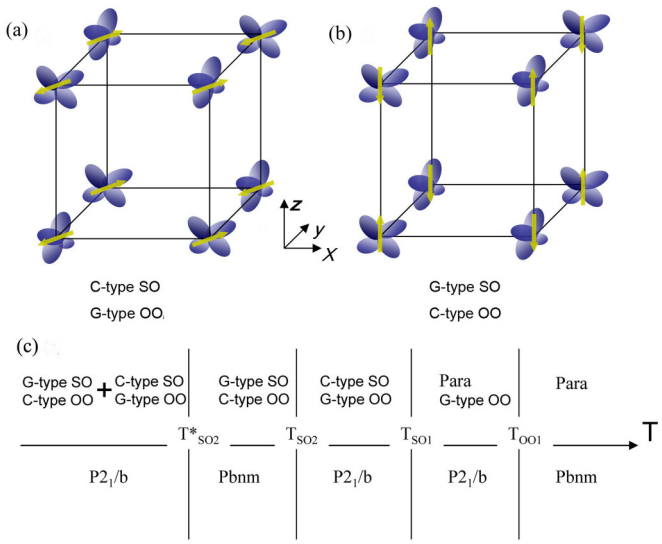

FIG. 1. (Color online) Schematic view of (a) C-type spin ordering (SO) with G-type orbital ordering (OO) and (b) G-type SO with C-type OO of $DyVO_3$. The yellow arrows and blue lobes denote spins and occupied orbitals of the V^{3+} ions, respectively. (c) Summary of the sequence of structural, spin-, and orbital-ordering transitions in $DyVO_3$, based on previous reports [27,29,32–36].

of the R^{3+}-ion radius [33] and also at the phase boundary between the two competing spin-orbital-ordered states [33], a peculiarity which makes its structural and physical properties very complex below T_{SO1}. On the basis of previous studies [27,29,32–36], the sequence of the transitions affecting the spin, orbital, and lattice degrees of freedom in $DyVO_3$ is summarized in Fig. 1(c). The G-type OO state in $DyVO_3$ evolves to C-type OO below T_{SO2} (55–62 K) [27,30,35] with the alternate $d^1_{xy}d^1_{yz}/d^1_{xy}d^1_{zx}$ electron configuration in the xy plane and the same one along the z axis and the structure changes back to the $Pbnm$ orthorhombic structure again. Simultaneously, the C-type SO reorients into G-type SO at T_{SO2} with an AFM coupling between the V^{3+} moments ($\| c$) in all three directions [see Fig. 1(b)]. In addition, $DyVO_3$ [27,34,36] exhibits an additional reentrant transition to C-type SO/G-type OO and a structural transition from $Pbnm$ orthorhombic to $P2_1/b$ monoclinic as the temperature is lowered below T^*_{SO2} (18–22 K). It should be noted that recent x-ray and Raman scattering experiments [27] have shown that the volume fraction of the C-type SO/G-type OO state below T^*_{SO2} is only about 1/3 and that the rest remains in the G-type SO/C-type OO state, resulting in a phase coexistence state below T^*_{SO2}. Motivated by the particular richness of the spin- and orbital-ordering processes encountered in $DyVO_3$ crystal, we have selected this system to investigate the possible occurrence of multiferroic behavior in the RVO_3 family.

II. EXPERIMENTAL DETAILS

The $DyVO_3$ crystals have been grown with the floating-zone method using a high-temperature xenon arc furnace. The details of the crystal growth are similar to those reported previously for other RVO_3 crystals [31,37]. The crystalline orientation was confirmed by using back-reflection x-ray Laue photographs. The temperature/field dependence of magnetization for $H \| b$ and resistivity were recorded by means of a physical properties measurement system (PPMS, Quantum Design). Heat capacity measurements were carried out in the same PPMS using a semiadiabatic relaxation method.

The complex dielectric permittivity was measured on a parallel plate capacitor geometry and silver-paste electrodes were made on two different capacitors to apply an electric field along the c or the b axis and the magnetic field is applied along the b axis. The dielectric permittivity ε' and the losses $\tan\delta$ were measured using an Agilent 4284 A LCR meter during both cooling and warming processes (0.5 K/min) with a 0.5 V ac bias field at different frequencies (5–100 kHz). The electric polarization with $E \| b$ was measured with a Keithley 6517 A electrometer in a Coulomb mode with automatic current integration facility.

To align the ferroelectric domains, a static electric poling field of +400 kV/m was applied along the b or the c axis during cooling from 120 K down to 8 K. After this poling field was removed at 8 K, we did short circuit and charge was recorded as a function of time for 6400 s at 8 K to reach a stable state and to remove possible stray or trapped charge. The detailed experimental procedure and related experimental data can be found in the Supplemental Material [38]. The temperature dependence of electric polarization (P) was subsequently recorded during warming (0.5 K/min) in zero electric field. After this, the direction of static electric poling field was changed (−400 kV/m) and the same experimental procedure was carried out to measure the temperature dependence of the electric polarization with $E \| b$. As known, the polarizations in the type-II multiferroics are usually typically three to four orders of magnitude lower traditional ferroelectricity, like $10^2\ \mu C/cm^2$ in $BiFeO_3$ [39], and the coercive electric fields in such type-II multiferroics are usually very high, which makes the $P(E)$ hysteresis loop measurements hardly achieved. Thus, the above experimental procedure and the symmetric reversal of P upon reversing the poling electric field are widely used ways to check the presence of ferroelectric polarization, as has been adopted in many previous reports [17,18,21,22,39,40]. We have also measured the resistivity and dielectric loss and paid cautious attention to exclude other possible contributions, such as leakage contribution or trapped charge, as discussed in the text.

III. RESULTS AND DISCUSSION

A. Magnetic properties

The temperature dependence of the field-cooled-cooling (FCC) and field-cooled-warming (FCW) magnetization of $DyVO_3$ in a magnetic field of 20 Oe parallel to the b axis is shown in Fig. 2(a). There is an increase in magnetization at $T_{SO1} \sim 108$ K for both the FCC and the FCW processes, corresponding to a magnetic transition from paramagnetic (PM) to AFM C-type SO transition [27,34,36]. The increase of magnetization at T_{SO1} has been reported to reflect the spin canting of V moments related to the antisymmetric Dzyaloshinskii-Moriya (DM) interaction [33,36]. Note that for the RVO_3 compounds with small ionic radius such as Dy, Y, Ho, and Er, a weak z component of the G type exists along with the previously reported strong C modes in the

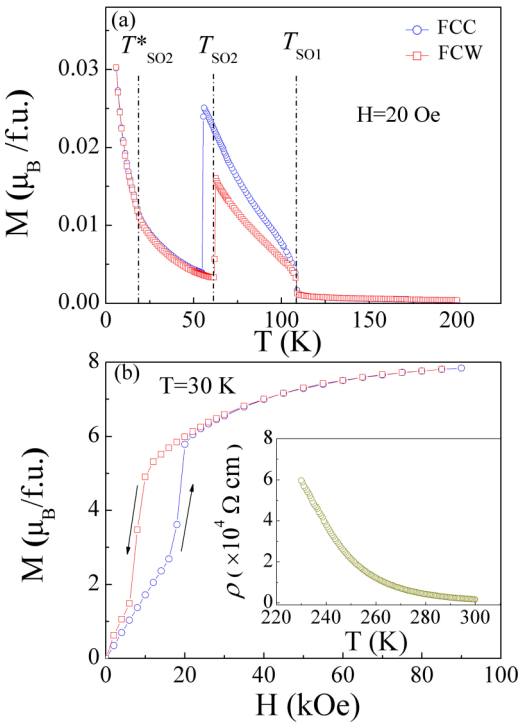

FIG. 2. (Color online) (a) Temperature dependence of the FCC and FCW magnetization of $DyVO_3$ in a field of 20 Oe parallel to the b axis, with dashed lines marking the three transitions. (b) Magnetization curve with $H \parallel b$ at 30 K as the field is ramped up and down (see arrows). The inset shows the temperature dependence of the resistivity of $DyVO_3$ in zero magnetic field.

xy plane [29,33,36,37,41–43]. Thus, the magnetic structure below T_{SO1} in these systems is not purely collinear C-type SO. Instead, the AFM-aligned V $3d$ spins are a superposition of C modes in the xy components (AFM alignment in the xy plane and ferromagnetic alignment along the z axis) and the weakest G-type order of the z component, forming noncollinear vanadium spins with $CxCyGz$ mode in $DyVO_3$ [29,33,36–42]. Upon decreasing the temperature to T_{SO2}, a rapid decrease in the magnetization along the b axis takes place for both the FCC and the FCW process. This is ascribed to the reorientation [27,34] from C-type SO to collinear G-type SO with the V spins parallel to the z axis, the latter configuration being not expected to favor large spin canting. There is a significant thermal hysteresis around T_{SO2} between the FCC and the FCW magnetization curves, indicating that this transition is first order. The transition temperature is found to be 55.2 K and 62.3 K in the cooling and warming process, respectively. The thermal hysteresis of 7 K is in line with the results (57 and 64 K) reported by Miyasaka *et al.* [34]. For the sake of simplicity, we will only use the value (~62 K) for the warming process in the rest of the paper. Around T^*_{SO2} (~18 K), the magnetization increases rapidly and there is a change in the slopes of the magnetization as well as an anomaly in the inverse susceptibility (not shown), which shows a reentrant transition from G-type SO/C-type OO to C-type SO/G-type OO [27,34]. These magnetic characterizations in the present crystal are consistent with previous reports [27,34]. It is worthwhile noting that the Dy moments have been reported to become fully ordered below T^*_{SO2} [41]. The increase of the magnetization at T^*_{SO2} is therefore due to the combined contribution from the spin canting of the V spins and the ordered Dy moments.

In the temperature region between T^*_{SO2} and T_{SO2}, a field-induced metamagnetic transition from G-type SO/C-type OO to C-type SO/G-type OO is observed in $DyVO_3$, as can be seen in the representative isothermal magnetization curve at 30 K with $H \parallel b$ in Fig. 2(b). For the virgin curve, the magnetization starts to increase rapidly around a threshold field Ht (~1.6 T) due to the metamagnetic transition [27,33,34,36] from G-type SO/C-type OO to more stable C-type SO/G-type OO, a magnetic order in which spin canting allows a larger net magnetization to be reached in a magnetic field [36]. A large magnetic hysteresis is observed as the field is ramped up and down, marking again the first-order nature of the transition between G-type SO/C-type OO and C-type SO/G-type OO. Since the maximum magnetic moment of V $3d$ is only $2\mu_B$, the high saturation magnetization of around $8\mu_B$ reached above Ht suggests that the field-induced spin/orbital transition occurs concomitantly with the polarization of Dy $4f$ moments by the external field, which can be explained by the coupling between the Dy $4f$ and the V $3d$ spins [27]. In addition, the high saturation magnetization for $H \parallel b$ suggests that the b axis is an easy magnetization direction, in accordance with Refs. [27,34], in which both a and b axes were reported to be easy axes, while the c axis is magnetic hard axis.

B. Heat capacity

The temperature dependence of $Cp(T)$/T below 180 K in zero magnetic field for the warming process is shown in Fig. 3. The peak at 108 K marks T_{SO1}, while the rapid decrease at 62 K with decreasing temperature corresponds to T_{SO2}. Another anomaly can be observed at 18 K (see inset of Fig. 3), which marks the reentrant transition temperature T^*_{SO2}. The three transition temperatures are in good agreement with the values observed in the magnetization measurements. The present heat capacity results are different from those reported in Ref. [29], where no anomaly is observed at T^*_{SO2}. We suggest that, as

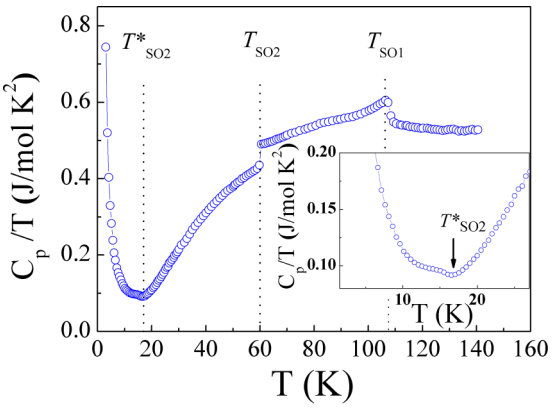

FIG. 3. (Color online) Temperature dependence of the ratio C_p/T for $DyVO_3$ in zero field during the warming process with dashed lines marking the three transitions. The inset shows an enlargement of C_p/T around T^*_{SO2}.

compared with T_{SO2}, the weaker anomaly in Cp(T) at T^*_{SO2} should be ascribed to the incomplete spin/orbital transition, as mentioned above. In contrast, at T_{SO2}, the C-type SO/G-type OO state transforms completely to pure G-type SO/C-type OO, leading to a sharp jump in Cp(T)/T. Similar features are observed in the dielectric properties, as will be shown below.

C. Resistivity, dielectric permittivity, and loss

The resistivity of $DyVO_3$ is found to increase rapidly with decreasing temperature [see inset of Fig. 2(b)] without the magnetic-field-induced magnetoresistance effect. At 227 K, the resistivity is already as high as 6×10^4 Ω cm (resistance is 4.3×10^5 Ω), suggesting that the resistivity of $DyVO_3$ below 120 K is far higher than this magnitude. Figures 4(a) and 4(b) present the temperature dependence of dielectric permittivity ε' during the warming process at 5 kHz with ac bias $E \parallel b$ and $E \parallel c$, respectively. One weak kink with a slope change corresponding to a peak in the first derivative of the $\varepsilon'(T)$ curve [see the insets in Figs. 4(a) and 4(b)] is observed around T_{SO1} with $E \parallel b$ and $E \parallel c$. When the frequency increases to 100 kHz, the kink in the $\varepsilon'(T)$ curve evolves to one concave cusp, as shown in Figs. 5(a) and 5(c). Such type of dielectric anomaly [a change of slope or a peak in $d\varepsilon'(T)/dT$] has been reported at the ferroelectric critical temperature for many spin-driven ferroelectricities, such as $Ca_3Co_{2-x}Mn_xO_6$ ($x = 0.96$) [44], ACr_2O_4 (A = Fe or Cr) [17], FeV_2O_4 [18], and $RCrO_3$ (R = Sm, Gd, Tb, Er, and Tm) [21]. As also shown in Figs. 5(a) and 5(c), a rapid jump in ε' and a large thermal hysteresis between cooling and warming processes around T_{SO2} mark the first-order transition. We point out that ε' is not superimposed mainly above T_{SO2} for cooling and warming processes. The exact origin of this feature is not clear, but this is probably ascribed to the influence of such first-order transition at T_{SO2} after the different thermal processes. In addition, a kink is also observed at T^*_{SO2} (= 18 K) with $E \parallel b$ and $E \parallel c$. Note that the locations of these three anomalies in ε' are frequency independent (not shown) and coincide well with the three transitions observed in the magnetization and heat capacity measurements.

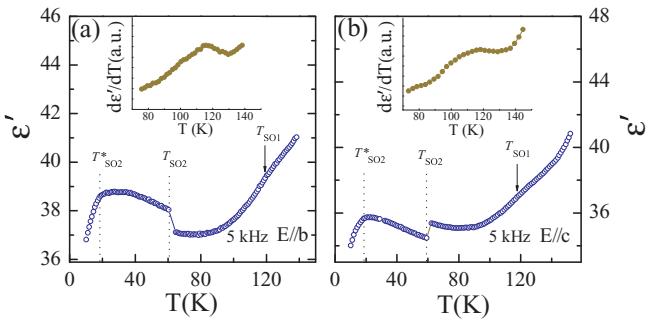

FIG. 4. (Color online) Temperature dependence of the dielectric permittivity with (a) $E \parallel b$ and (c) $E \parallel c$ for $DyVO_3$, measured at a low frequency of 5 kHz for the warming process. The insets of (a) and (b) show the corresponding first derivative of the dielectric permittivity as a function of temperature. The dashed lines and the arrow show the locations of the three transitions T_{SO1}, T_{SO2}, and T^*_{SO2}.

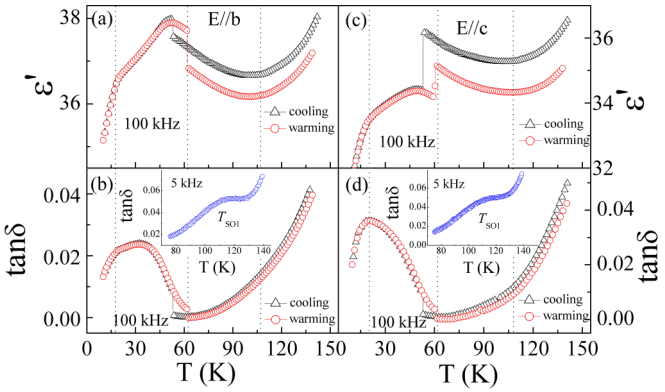

FIG. 5. (Color online) Temperature dependence of the dielectric permittivity and dielectric loss (tanδ) with $E \parallel b$ [(a), (b)] and $E \parallel c$ [(c), (d)] for $DyVO_3$, measured at 100 kHz for both cooling and warming processes. The insets of (b) and (d) show the clear rise of tanδ at T_{SO1} at a low frequency of 5 kHz. The three dashed lines mark the three transitions T_{SO1}, T_{SO2}, and T^*_{SO2} with decreasing temperature.

It is worthwhile pointing out that the value of the dielectric loss in dielectric measurements reflects the insulating behavior of the sample. For a real capacitor (good insulator), the value of tanδ should be close to zero. The temperature dependence of the dielectric loss (tanδ) recorded at 100 kHz is shown in Figs. 5(b) and 5(d). At 120 K, the value of tanδ is quite low (≈0.02) for $E \parallel b$ or c and further decreases close to zero, followed by a weak increase with decreasing temperature. Combining the very low dielectric loss with the resistivity measurements [see the inset of Fig. 2(b)], we can conclude that $DyVO_3$ is highly insulating below ≈120 K. Moreover, the locations of three anomalies in ε' are frequency independent. Thus, we can exclude possible extrinsic factors [20], such as trapped interfacial charge carriers, and state that these measurements reflect intrinsic electric transitions at T_{SO1}, T_{SO2}, and T^*_{SO2}. In addition, the anomalies at T_{SO1}, T_{SO2}, and T^*_{SO2} are also found in the tanδ vs T curve, for both the warming and the cooling process [see Figs. 5(b) and 5(d)]. Note that the formation of electric dipoles leads to an increase in the dielectric loss at T_{SO1}, which can be seen more clearly under a low frequency, such as 5 kHz in the insets of Figs. 5(b) and 5(d). Although there are no clear differences in the locations of the three anomalies in the $\varepsilon'(T)$ curve with $E \parallel b$ and $E \parallel c$, ε' shows anisotropic behavior at T_{SO2}, i.e., a rapid decrease of ε' for $E \parallel c$ in contrast with a rapid increase for $E \parallel b$ during cooling, exhibiting the anisotropic features of the dielectric properties. It is worthwhile pointing out that one observes another broad hump in tanδ which is centered around ∼36 K for $E \parallel b$, but this feature is absent for $E \parallel c$, which further indicates the anisotropic character of the dielectric properties of $DyVO_3$.

To study the effect of a magnetic field on the dielectric properties, we have measured ε' vs T at 100 kHz in a small magnetic field of 5 kOe parallel to the b axis for both orientations ($E \parallel b$ and $E \parallel c$), as shown in Figs. 6(a) and 6(b). Interestingly, a clear effect of magnetic field on ε' is observed at T_{SO1}, i.e., a sudden H-induced dip in ε' for $E \parallel b$. In addition, a small magnetic field of 5 kOe shifts the anomaly

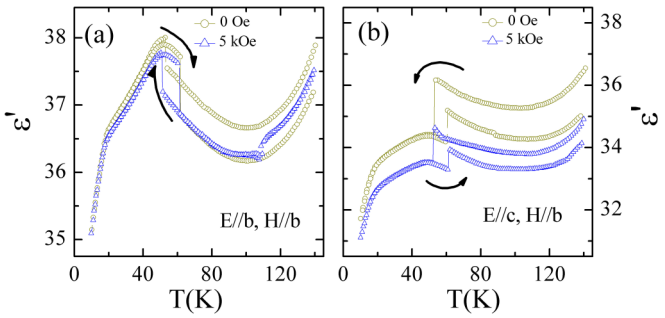

FIG. 6. (Color online) Temperature dependence of the dielectric permittivity of $DyVO_3$ in zero magnetic field and in a magnetic field of 5 kOe parallel to the b axis with (a) $E \parallel b$ and (b) $E \parallel c$.

at T_{SO2} slightly to lower temperatures (~1 K) for $E \parallel b$. No such effects are observed for $E \parallel c$, which implies the possible anisotropic effect of magnetic field on ε'.

D. Electric polarization with multiple anomalies

To investigate the presence of ferroelectricity, we have measured the temperature dependence of electric polarization (P) with an electrometer directly in the Coulombic mode with E parallel to the b and c axes. The detailed measurement procedure and related experimental data can be found in the "Experimental Details" section and in the Supplemental Material. As shown in Fig. 7, one observes the appearance of polarization in $DyVO_3$ below the magnetic transition at T_{SO1} for $E \parallel b$ or $E \parallel c$, a feature pointing to the magnetic origin of the ferroelectricity in this system. With decreasing temperature, two additional anomalies can be detected in the $P_b(T)$ curve around T_{SO2} and around 36 K, corresponding to the two peaks in the first derivative of P_b (dP_b/dT) [see inset of Fig. 7(a)]. One can also observe an anomaly in $P_c(T)$ around T_{SO2}. However, there is no clear anomaly in $P_c(T)$ around 36 K and an additional decrease in the electric polarization is only observed below T^*_{SO2} in $P_c(T)$ as shown in Fig. 7(b). This overall behavior demonstrates a close interplay between the nature of the spin/orbital ordering and the ferroelectric properties. The remnant polarization values along the b and c axes are 320 and 700 $\mu C/m^2$, respectively.

Much cautious attention has been paid to exclude any artifact effect and confirm the ferroelectricity. The electrical current i between the two electrodes attached on a parallel plate can be given as [45]

$$i = C\frac{dV}{dt} + A\frac{dP}{dt} + \frac{V}{R}, \quad (1)$$

where V is applied voltage, $C = \varepsilon\varepsilon_0 A/L$ is the capacitance, A is contact area and L is the thickness of the crystal, P is the ferroelectric polarization, and R is the sample resistance. The three terms in Eq. (1) from left to right are the capacitive, ferroelectric, and resistive currents, respectively. The high-insulating behavior below ≈120 K excludes significant resistive current and the high resistance without the magnetoresistance effect also excludes the influence of the Maxwell-Wagner effect in $DyVO_3$. Moreover, the current and voltage phase angle derived from the very low dielectric loss in the dielectric measurements is around −89°, corresponding

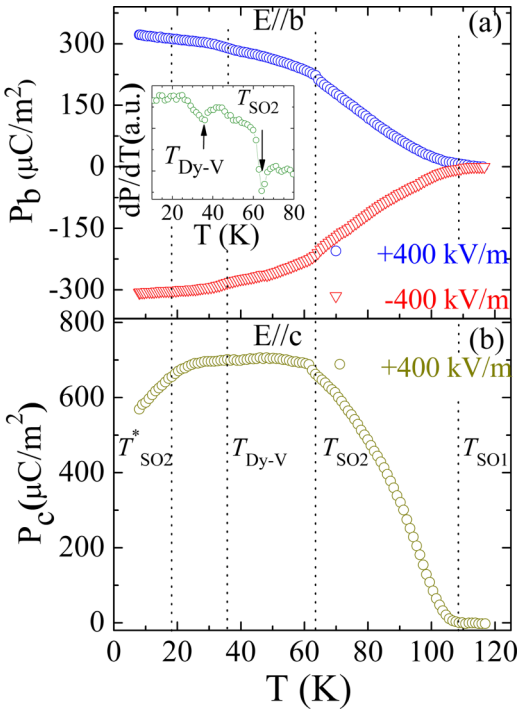

FIG. 7. (Color online) (a) Temperature dependence of the electric polarization (P_b) of $DyVO_3$, recorded during warming (0.5 K/min) after applying a static electric poling field of +400 or −400 kV/m parallel to the b axis. (b) Temperature dependence of the electric polarization (P_c) in $DyVO_3$, after using a static electric poling field of +400 kV/m parallel to the c axis. The inset of Fig. 7(a) shows the corresponding dP_b/dT curve derived from the measurements after applying a positive poling field.

to the ideal value of a perfect capacitor. In addition, we have done short circuit and measured charge as a function of time for long time (6400 s) to remove stray or trapped charge (if any) and to reach a stable state prior to the P vs T measurements. This procedure safely excludes a possible contribution from leakage contribution or trapped charge to pyroelectric current [17,18,39,40,45,46]. The P vs T measurements have been conducted at zero bias voltage with increasing temperature to exclude the capacitive current and any artifact resulting from the variation of the electric field [45,46]. It must also be emphasized that reversing the poling electric field leads to a symmetric negative polarization indicative of switchable polarization [see Fig. 7(a)], which further confirms [17,18,21,22,40] the ferroelectric polarization below T_{SO1} (≈108 K) in $DyVO_3$. Note that the ferroelectricity in $DyVO_3$ takes place below a high temperature of 108 K (well above liquid nitrogen temperature) and exhibits substantial remnant polarization reaching ~700 $\mu C/m^2$ for $E \parallel c$ (with $E = 400$ kV/m). The saturation polarization is expected to be higher at high poling electric fields.

E. Origin of the ferroelectricity in $T_{SO2} < T < T_{SO1}$ and 36 K $< T < T_{SO1}$

Below T_{OO1} (~195 K), the G-type OO is formed with the orthorhombic- monoclinic structural transition, which, however, does not induce the electric polarization. The electric

polarization only emerges below T_{SO1}, where the G-type OO and fundamental structure are unchanged and only the spin ordering changed from paramagnetic to long-range-ordered C-type SO, which indicates that the presence of ferroelectricity below T_{SO1} is mainly driven by the spin ordering and therefore, $DyVO_3$ belongs to type-II multiferroics. As mentioned above, the V^{3+} magnetic moments exhibit noncollinear ordering with the modes $CxCyGz$ [36–42] in the temperature region $T_{SO2} < T < T_{SO1}$. It has been established that the origin of polarization in the noncollinear magnetic structure can be explained by the $\boldsymbol{S}_i \times \boldsymbol{S}_j$-type spin-current model or the antisymmetric DM interaction [6,18,47]. Such model has successfully explained the origin of polarization in many noncollinear magnetic systems [10,13–18,47,48]. Recently, Kaplan [49] has further developed the conventional spin-current model by adding additional terms which were omitted previously in the existing microscopic models. It has been demonstrated that a pair of magnetic atoms with canted spins $\boldsymbol{S}_i$ and $\boldsymbol{S}_j$ can give rise to a relatively large electric dipole moment $\boldsymbol{P}$. Thus, in $DyVO_3$, based on the (extended) spin-current model, the noncollinear V $3d$ spins in $DyVO_3$ with weak spin canting due to the existing antisymmetric DM exchange interaction [36] imposed to the monoclinic $P2_1/b$ space group probably contribute to some extent to the polarization along the b and c axes in the temperature interval $T_{SO2} < T < T_{SO1}$.

However, the case here is not so simple. In the temperature region of 36 K $< T < T_{SO2}$, the noncollinear C-type SO reorients into collinear G-type SO and simultaneously, the G-type OO switches to C-type OO. The (extended) spin-current model cannot predict the polarization due to the collinear V^{3+} magnetic structure in the purely G-type SO. It should be noted that the magnetic structures change from C-type SO to G-type SO in $DyVO_3$ at T_{SO2}, but the direction of the electric polarization does not change despite the different spin orientation (see Fig. 7), which is an indication [50] that the $\boldsymbol{S}_i \cdot \boldsymbol{S}_j$-type exchange-striction mechanism plays an important role in the polarization throughout T_{SO2}, i.e., not only below T_{SO2}, but also above T_{SO2}. This is in contrast with the spin-current model, based on which the direction of P is strongly dependent on the direction of $\boldsymbol{S}_i \times \boldsymbol{S}_j$. It has been discussed that the ferroelectricity could be induced by the PM-AFM transition in the centrosymmetric crystals belonging to space groups, such as $Pmma$, $Pbnm$, $Pbam$, etc. [51]. The AFM transition doubles the unit cell and makes such crystals lose their center of symmetry, leading to a noncentrosymmetric point group and inducing the ferroelectricity by the exchange-striction mechanism. In $DyVO_3$, the long-range AFM C-type (or G-type) SO of the V spins is imposed with the centrosymmetric space group $P2_1/b$ (or $Pbnm$) below T_{SO1}, which provides a possibility to lower the symmetries and induce the noncentrosymmetric point group. Furthermore, the real symmetry in most RVO_3 systems would be lower due to pronounced octahedral tilting [30,35]. Recently, it is argued [30,42] that the symmetry of the G-type OO phase in the RVO_3 family is lower than the generally accepted $P2_1/b$, most likely being noncentrosymmetric monoclinic $Pb11$, as observed by both optical [42,52] and neutron spectroscopy [53] on YVO_3 single crystals. The lower symmetry of $Pb11$ allows the possibility of V-V dimerization along the c axis that is consistent with the tentative identification of an "orbital Peierls state" [42,53] in YVO_3 and also accords to the existence of orbital fluctuations in the monoclinic phase in the RVO_3 family [30,54–56]. It turns out that it is hard [42] to distinguish $Pb11$ and $P2_1/b$ only from the synchrotron x-ray or neutron diffraction measurements in RVO_3 systems since the monoclinic distortion in these systems is extremely small. Similar optical and neutron spectroscopy experiments performed on YVO_3 [52,53] are required to distinguish $Pb11$ and $P2_1/b$ in the monoclinic phase in $DyVO_3$ and other RVO_3 compounds. All these features support the appearance of ferroelectricity via exchange-striction below T_{SO1} in $DyVO_3$. In this scenario, the magnetic interactions between adjacent V spin pairs modify the V-O-V bond angle/length and induce the oxygen polarization via $\boldsymbol{S}_i \cdot \boldsymbol{S}_j$-type exchange striction, which leads to the macroscopic ferroelectricity in $DyVO_3$. The magnitude of magnetic exchange coupling J [6,57,58] depends on the orbital occupancy and thereby on the shape and orientation of these orbitals. Such scenario is similar to the interpretation of observation of polarization in orthomanganite $HoMnO_3$ [57,59], and spinel CdV_2O_4 [60], where an AFM ordering of the transition-metal Mn or V spins imposed to the fundamentally centrosymmetric space groups. Thus, whereas the exchange striction plays a main role in the presence of ferroelectric polarization below T_{SO1}, the extended spin-current model cooperates [6,10,61,62] with the exchange striction mechanism to contribute to the polarization in $T_{SO2} < T < T_{SO1}$.

F. Origins of the anomalies at 36 K and T^*_{SO2} in the ferroelectricity

When the temperature further decreases, an additional weak anomaly is observed only in the $P_b(T)$ curve at 36 K, which is higher than T^*_{SO2}. This is in good agreement with the dielectric measurements, i.e., a hump for $E \parallel b$ but no anomaly for $E \parallel c$ in the $\tan\delta$ (T) curve at the same temperature of 36 K. Neutron diffraction experiments [41] suggest that, for the warming process, the Dy moments are long-range ordered with F_xC_y mode fully below T^*_{SO2} and then C_xF_y mode below 13 K. However, a common physical picture for the RVO_3 family is that the moments of the lanthanide ions are gradually polarized by the ordered V moments via R-V coupling at temperatures above the full ordering temperature of the R^{3+} sublattice via R-R coupling. For example, in $CeVO_3$, Ce becomes ordered at 28 K, whereas the polarization of the Ce moments starts at about 60 K [63]. In $NdVO_3$, the Nd moments are slightly induced by V moments between 60 and 9.5 K, and then become full ordered at 9.5 K [42]. For $TbVO_3$, the ordering of the Tb moments with the C_xF_y mode emerges at 11 K, whereas slight ordering of the Tb moments via Tb-V coupling starts at 40 K [27,42]. A similar polarization process of rare-earth moments has been observed earlier in other perovskites, such as $NdFeO_3$ [64], and also in iron-pnictide CeFeAsO [65]. Thus, the induced ordering of Dy moments probably takes place at 36 K due to Dy-V coupling. The absence of direct observation on the slight polarization of Dy moment around 36 K in $DyVO_3$ by neutron diffraction may be ascribed to the large neutron absorption cross section of Dy ions, as suggested by Reehuis *et al.* in Ref. [41]. However,

they have observed slight ordering of the Tb moments at 40 K from the anomaly in the temperature dependence of magnetic reflections of $TbVO_3$ involving the weaker neutron absorption cross section of Tb ions [42]. Since the Tb-V and the Dy-V couplings are comparable in orthovanadates, it is reasonable that the onset of slight polarization of the lanthanide ions may occur at similar temperatures, i.e., at 40 K in $TbVO_3$ and at 36 K in $DyVO_3$. The temperature-induced reentrant transition at T^*_{SO2} and the field-induced switching from G-type SO/C-type OO to C-type SO/G-type OO accompanied by a rapid increase of the Dy moments imply possible exchange coupling between the V $3d$ spins and the Dy $4f$ moments [27,33,34]. Since the long-range Dy ordering (F_xC_y or C_xF_y) only takes place in the ab plane [41] without a component along the c axis, the possible partially polarized Dy spins below 36 K would be confined to the ab plane. It is well known that ordering of rare-earth moments plays a significant role in inducing the emergence or the anomaly of ferroelectricity, like in $HoMnO_3$ [45], $TmMn_2O_5$ [10], $GdFeO_3$ [50], and $DyFeO_3$ [66]. Thus, the gradually polarized Dy moments in the ab plane by the V moments below T_{Dy-V} ($\approx$36 K) gives rise to an additional ferroelectric distortion via the exchange-striction mechanism besides the contribution from the V spin order, which results in a weak increase of P_b with respect to temperature. Since there are no partially polarized Dy spins along the c axis, this might account for the absence of an anomaly in the $P_c(T)$ curve around 36 K.

As temperature further decreases to T^*_{SO2} (=18 K), the electric polarization decreases only for $E \parallel c$, suggesting that the concomitant occurrence of a reentrant transition from G-type SO/C-type OO to C-type SO/G-type OO in V sublattice and the emergence of long-range Dy ordering also influences the ferroelectricity via the exchange striction mechanism. It has come to our attention that very recently, Rajeswaran *et al.* [21] proposed another interesting scenario related to the exchange-striction mechanism to explain the presence of ferroelectricity below Néel temperature of Cr sublattice in rare-earth orthochromites $RCrO_3$ (R = Sm, Gd, Tb, Er, and Tm) with the centrosymmetric space group $Pbnm$. The poling procedure induces small distortion of R ions and their surrounds, and the interplay between R and Cr providing isotropic Heisenberg-like exchange striction, reinforces such initial distortion, leading to the emergence of ferroelectricity below Néel temperature. This scenario may also be applicable for interpreting the presence of the ferroelectricity below Néel temperature T_{SO1} in our orthovanadate $DyVO_3$. It should be pointed out that the exact microscopic coupling between electric dipoles and spins over a wide temperature range below the Néel temperature T_{SO1} in $DyVO_3$ is unclear due to the complex and numerous competing magnetic exchange interactions in this system. However, we believe the exchange-striction mechanism among V spins and/or between Dy and V spins plays a major role in the presence of electric polarization with the multiple anomalies with respect to temperature below T_{SO1} in $DyVO_3$. In consideration of the relatively small magnitude of the electric polarization in $DyVO_3$, high-resolution x-ray techniques performed on orthorhombic $RMnO_3$ (R = Y [67] or Tb [68]) and/or the *ab initio* calculation is required to study the ionic displacements of oxygen and/or dysprosium and their temperature dependence in order to reveal the exact microscopic origin of the ferroelectricity with multiple anomalies in $DyVO_3$.

IV. CONCLUSION

In summary, the orthovanadate $DyVO_3$ is found to be a new type-II multiferroic material with a high critical temperature of 108 K and very low dielectric loss. The onset of electric polarization along the b or c axis concurs with the PM-AFM C-type SO transition, where a peak in the heat capacity and an anomaly in the dielectric permittivity are also observed. With decreasing temperature, the $P_b(T)$ curve exhibits two additional anomalies at T_{SO2} (=62 K) and at 36 K, which correspond to transition from C-type SO/G-type OO to G-type SO/C-type OO and the possible onset of polarized Dy moments, respectively. While one anomaly in $P_c(T)$ is also observed at T_{SO2} no anomaly is observed around 36 K and another decrease in $P_c(T)$ is found below T^*_{SO2} ($\sim$18 K). The high critical temperature, low dielectric loss, and the coupled magnetism and ferroelectricity make $DyVO_3$ an interesting multiferroic material. The present study may attract the attention of experimentalists and theorists to investigate the possibility of more high-temperature multiferroics and explore the exact microscopic origin of the ferroelectricity in the RVO_3 (R = rare-earth elements, especially with a relatively small ionic radius such as Gd, Tb, Ho, Er, Yb, and Lu) single crystals.

ACKNOWLEDGMENTS

This work has been supported by the European project "SOPRANO" under Marie Curie actions (Grant No. PITNGA-2008-214040) and French project "PR Refrigeration Magnétique." We thank F. Guillou for his instructions on the heat capacity measurements, L. Hervé for aligning single crystal in different orientations, and also F. Veillon for the resistivity measurements.

[1] T. Lottermoser, T. Lonkai, U. Amann, D. Hohlwein, J. Ihringer, and M. Fiebig, Nature (London) **430**, 541 (2004).
[2] P. J. Ryan, J.-W. Kim, T. Birol, P. Thompson, J.-H. Lee, X. Ke, P. S. Normile, E. Karapetrova, P. Schiffer, S. D. Brown, C. J. Fennie, and D. G. Schlom, Nat. Commun. **4**, 1334 (2013).
[3] Q. Zhang, C. H. Kim, Y. H. Jang, H. J. Hwang, and J. H. Cho, Appl. Phys. Lett. **96**, 152901 (2010).
[4] G. Catalan and J. F. Scott, Adv. Mater. **21**, 2463 (2009).
[5] D. A. Sanchez, N. Ortega, Ashok Kumar, R. Roque-Malherbe, R. Polanco, J. F. Scott, and Ram S. Katiyar, AIP Adv. **1**, 042169 (2011).
[6] T. Arima, J. Phys. Soc. Jpn. **80**, 052001 (2011); S. Ishihara, *ibid.* **79**, 011010 (2010).
[7] S. Dong and J.-M. Liu, Mod. Phys. Lett. B **26**, 1230004 (2012).
[8] E. Ascher, H. Schmid, and D. Tar, Solid State Commun. **2**, 45 (1964); H. Schmid, Ferroelectrics **162**, 317 (1994).

[9] R. E. Newnham, J. J. Kramer, W. A. Schulze, and L. E. Cross, J. Appl. Phys. **49**, 6088 (1978).

[10] M. Fukunaga, Y. Sakamoto, H. Kimura, Y. Noda, N. Abe, K. Taniguchi, T. Arima, S. Wakimoto, M. Takeda, K. Kakurai, and K. Kohn, Phys. Rev. Lett. **103**, 077204 (2009).

[11] H. Kimura, S. Kobayashi, Y. Fukuda, T. Osawa, Y. Kamada, Y. Noda, I. Kagomiya, and K. Kohn, J. Phys. Soc. Jpn. **76**, 074706 (2007).

[12] Y. Noda, H. Kimura, M. Fukunaga, S. Kobayashi, I. Kagomiya, and K. Kohn, J. Phys.: Condens. Matter **20**, 434206 (2008).

[13] I. Cabrera, M. Kenzelmann, G. Lawes, Y. Chen, W. C. Chen, R. Erwin, T. R. Gentile, J. B. Leao, J. W. Lynn, N. Rogado, R. J. Cava, and C. Broholm, Phys. Rev. Lett. **103**, 087201 (2009).

[14] A. Dixit and G. Lawes, J. Phys.: Condens. Matter **21**, 456003 (2009); A. Daoud-Aladine, B. Kundys, C. Martin, P. G. Radaelli, P. J. Brown, C. Simon, and L. C. Chapon, Phys. Rev. B **80**, 220402(R) (2009); L. Zhao, M. P. Y. Wu, K. W. Yeh, and M. K. Wu, Solid State Commun. **151**, 1728 (2011).

[15] F. Ye, R. S. Fishman, J. A. Fernandez-Baca, A. A. Podlesnyak, G. Ehlers, H. A. Mook, Y. Wang, B. Lorenz, and C. W. Chu, Phys. Rev. B **83**, 140401(R) (2011).

[16] Y. Yamasaki, S. Miyasaka, Y. Kaneko, J. P. He, T. Arima, and Y. Tokura, Phys. Rev. Lett. **96**, 207204 (2006).

[17] K. Singh, A. Maignan, C. Simon, and C. Martin, Appl. Phys. Lett. **99**, 172903 (2011).

[18] Q. Zhang, K. Singh, F. Guillou, C. Simon, Y. Breard, V. Caignaert, and V. Hardy, Phys. Rev. B **85**, 054405 (2012); Q. Zhang, M. Ramazanoglu, S. Chi, Y. Liu, T. A. Lograsso, and D. Vaknin, *ibid.* **89**, 224416 (2014).

[19] S. Seki, Y. Onose, and Y. Tokura, Phys. Rev. Lett. **101**, 067204 (2008).

[20] L. Zhao, T.-L. Hung, C.-C. Li, Y.-Y. Chen, M.-K. Wu, R. K. Kremer, M. G. Banks, A. Simon, M.-H. Whangbo, C. Lee, J. S. Kim, I. Kim, and K. H. Kim, Adv. Mater. **24**, 2469 (2012).

[21] B. Rajeswaran, D. I. Khomskii, A. K. Zvezdin, C. N. R. Rao, and A. Sundaresan, Phys. Rev. B **86**, 214409 (2012).

[22] T. Kimura, Y. Sekio, H. Nakamura, T. Siegrist, and A. P. Ramirez, Nat. Mater. **7**, 291 (2008).

[23] R. D. Johnson, L. C. Chapon, D. D. Khalyavin, P. Manuel, P. G. Radaelli, and C. Martin, Phys. Rev. Lett. **108**, 067201 (2012).

[24] J.-H. Lee, Y. K. Jeong, J. H. Park, M.-A. Oak, H. M. Jang, J. Y. Son, and J. F. Scott, Phys. Rev. Lett. **107**, 117201 (2011).

[25] J.-H. Lee, Y. K. Jeong, J. H. Park, M.-A. Oak, H. M. Jang, J. Y. Son, and J. F. Scott, Phys. Rev. Lett. **108**, 219702 (2012).

[26] T. Sakai, G. Adachi, J. Shiokawa, and T. Shinike, J. Appl. Phys. **48**, 379 (1977).

[27] J. Fujioka, T. Yasue, S. Miyasaka, Y. Yamasaki, T. Arima, H. Sagayama, T. Inami, K. Ishii, and Y. Tokura, Phys. Rev. B **82**, 144425 (2010).

[28] J.-Q. Yan, J.-S. Zhou, and J. B. Goodenough, Phys. Rev. Lett. **93**, 235901 (2004).

[29] S. Miyasaka, Y. Okimoto, M. Iwama, and Y. Tokura, Phys. Rev. B **68**, 100406 (2003).

[30] M. H. Sage, G. R. Blake, C. Marquina, and T. T. M. Palstra, Phys. Rev. B **76**, 195102 (2007).

[31] L. D. Tung, M. R. Lees, G. Balakrishnan, and D. McK. Paul, Phys. Rev. B **75**, 104404 (2007).

[32] J.-Q. Yan, H. B. Cao, M. A. McGuire, Y. Ren, B. C. Sales, and D. G. Mandrus, Phys. Rev. B **87**, 224404 (2013).

[33] J. S. Zhou, J. B. Goodenough, J. Q. Yan, and Y. Ren, Phys. Rev. Lett. **99**, 156401 (2007).

[34] S. Miyasaka, T. Yasue, J. Fujioka, Y. Yamasaki, Y. Okimoto, R. Kumai, T. Arima, and Y. Tokura, Phys. Rev. Lett. **99**, 217201 (2007).

[35] G. R. Blake, T. T. M. Palstra, Y. Ren, A. A. Nugroho, and A. A. Menovsky, Phys. Rev. B **65**, 174112 (2002).

[36] J.-S. Zhou, J. B. Goodenough, J.-Q. Yan, J.-G. Cheng, K. Matsubayashi, Y. Uwatoko, and Y. Ren, Phys. Rev. B **80**, 224422 (2009).

[37] L. D. Tung, Phys. Rev. B **73**, 024428 (2006); L. D. Tung, M. R. Lees, G. Balakrishnan, and D. M. Paul, *ibid.* **76**, 064424 (2007).

[38] See Supplemental Material at http://link.aps.org/supplemental/10.1103/PhysRevB.90.024418 for the detailed experimental procedure and related experimental data (charge vs time) prior to the P vs T measurements.

[39] G. Q. Zhang, S. Dong, Z. B. Yan, Y. Y. Guo, Q. F. Zhang, S. J. Yunoki, E. Dagotto, and J.-M. Liu, Phys. Rev. B **84**, 174413 (2011).

[40] K. Singh, C. Simon, and P. Toledano, Phys. Rev. B **84**, 064129 (2011); B. Rajeswaran, P. Mandal, Rana Saha, E. Suard, A. Sundaresan, and C. N. R. Rao, Chem. Mater. **24**, 3591 (2012).

[41] M. Reehuis, C. Ulrich, K. Prokes, S. Mat'as, J. Fujioka, S. Miyasaka, Y. Tokura, and B. Keimer, Phys. Rev. B **83**, 064404 (2011).

[42] M. Reehuis, C. Ulrich, P. Pattison, B. Ouladdiaf, M. C. Rheinstadter, M. Ohl, L. P. Regnault, M. Miyasaka, Y. Tokura, and B. Keimer, Phys. Rev. B **73**, 094440 (2006).

[43] G. R. Blake, A. A. Nugroho, M. J. Gutmann, and T. T. M. Palstra, Phys. Rev. B **79**, 045101 (2009).

[44] Y. J. Choi, H. T. Yi, S. Lee, Q. Huang, V. Kiryukhin, and S.-W. Cheong, Phys. Rev. Lett. **100**, 047601 (2008).

[45] B. Lorenz, Y.-Q. Wang, and C.-W. Chu, Phys. Rev. B **76**, 104405 (2007).

[46] I. L. Guy and D. K. Das-Gupta, J. Appl. Phys. **70**, 5691 (1991).

[47] H. Katsura, N. Nagaosa, and A. V. Balatsky, Phys. Rev. Lett. **95**, 057205 (2005).

[48] S. Park, Y. J. Choi, C. L. Zhang, and S.-W. Cheong, Phys. Rev. Lett. **98**, 057601 (2007).

[49] T. A. Kaplan and S. D. Mahanti, Phys. Rev. B **83**, 174432 (2011).

[50] Y. Tokunaga, N. Furukawa, H. Sakai, Y. Taguchi, T. H. Arima, and Y. Tokura, Nat. Mater. **8**, 558 (2009).

[51] S. Goshen, D. H. Mukamel Shaked, and S. Shtrikman, Phys. Rev. B **2**, 4679 (1970).

[52] A. A. Tsvetkov, F. P. Mena, P. H. M. van Loosdrecht, D. van der Marel, Y. Ren, A. A. Nugroho, A. A. Menovsky, I. S. Elfimov, and G. A. Sawatzky, Phys. Rev. B **69**, 075110 (2004).

[53] C. Ulrich, G. Khaliullin, J. Sirker, M. Reehuis, M. Ohl, S. Miyasaka, Y. Tokura, and B. Keimer, Phys. Rev. Lett. **91**, 257202 (2003).

[54] G. Khaliullin, Prog. Theor. Phys. Suppl. **160**, 155 (2005).

[55] J.-Q. Yan, J.-S. Zhou, J. B. Goodenough, Y. Ren, J. G. Cheng, S. Chang, J. Zarestky, O. Garlea, A. Llobet, H. D. Zhou, Y. Sui, W. H. Su, and R. J. McQueeney, Phys. Rev. Lett. **99**, 197201 (2007).

[56] A. M. Oleś and P. Horsch, in *Properties and Applications of Thermoelectric Materials*, edited by V. Zlatić and A. C. Hewson, NATO Science for Peace and Security Series B (Springer, New York, 2009), pp. 299–324.

[57] N. Lee, Y. J. Choi, M. Ramazanoglu, W. Ratcliff, V. Kiryukhin, and S.-W. Cheong, Phys. Rev. B **84**, 020101(R) (2011).
[58] J. F. Scott, Europhys. Lett. **103**, 37001 (2013).
[59] I. A. Sergienko, C. Sen, and E. Dagotto, Phys. Rev. Lett. **97**, 227204 (2006).
[60] G. Giovannetti, A. Stroppa, S. Picozzi, D. Baldomir, V. Pardo, S. Blanco-Canosa, F. Rivadulla, S. Jodlauk, D. Niermann, J. Rohrkamp, T. Lorenz, S. Streltsov, D. I. Khomskii, and J. Hemberger, Phys. Rev. B **83**, 060402(R) (2011).
[61] M. Mochizuki, N. Furukawa, and N. Nagaosa, Phys. Rev. Lett. **105**, 037205 (2010).
[62] L. C. Chapon, P. G. Radaelli, G. R. Blake, S. Park, and S. W. Cheong, Phys. Rev. Lett. **96**, 097601 (2006).
[63] M. Reehuis, C. Ulrich, P. Pattison, M. Miyasaka, Y. Tokura, and B. Keimer, Eur. Phys. J. B **64**, 27 (2008).
[64] J. Bartolomé, E. Palacios, M. D. Kuz'min, F. Bartolomé, I. Sosnowska, R. Przeniosło, R. Sonntag, and M. M. Lukina, Phys. Rev. B **55**, 11432 (1997).
[65] Q. Zhang, W. Tian, H. Li, J.-W. Kim, J. Yan, R. W. McCallum, T. A. Lograsso, J. L. Zarestky, S. L. Bu'dko, R. J. McQueeney, and D. Vaknin, Phys. Rev. B **88**, 174517 (2013).
[66] Y. Tokunaga, S. Iguchi, T. Arima, and Y. Tokura, Phys. Rev. Lett. **101**, 097205 (2008).
[67] D. Okuyama, S. Ishiwata, Y. Takahashi, K. Yamauchi, S. Picozzi, K. Sugimoto, H. Sakai, M. Takata, R. Shimano, Y. Taguchi, T. Arima, and Y. Tokura, Phys. Rev. B **84**, 054440 (2011).
[68] H. C. Walker, F. Fabrizi, L. Paolasini, F. de Bergevin, J. Herrero-Martin, A. T. Boothroyd, D. Prabhakaran, and D. F. McMorrow, Science **333**, 1273 (2011).